(Received 28 May 2025, Accepted 3 August 2025, Scheduled 14 August 2025)

A Quasi-Yagi Antenna with Low Sidelobe and High Gain for the X-Band

Zhian Wang[1], Yunqi Zhang[1,*], Jianxiao Wang[2], Shanzhe Wang[1,4], Wenjia Zhou[1], Xinwei Wang[1], Leiyuan Wang[1], and Rong Zou[3]

[1]*School of Electronic Engineering, Xi'an University of Posts & Telecommunications, Xi'an 710121, China*
[2]*The National Key Laboratory of Science and Technology on Space Microwave China Academy of Space Technology, Xi'an 710100, China*
[3]*Hangzhou Institute of Technology, Xidian University, Hangzhou 311231, China*
[4]*National Key Laboratory of Automatic Target Recognition (ATR) College of Electronic Science and Technology National University of Defense Technology, Changsha 410073, China*

ABSTRACT: A compact quasi-Yagi antenna with ultra-wideband and high-gain characteristics is proposed. The design incorporates a conical dielectric cover, a horn reflector, and gradient-shaped Yagi elements. The conical dielectric cover and horn reflector work together to enable high-gain performance, while the arcuate gradient dipole provides a bandwidth of 62% (6.9–13.1 GHz). Measured results indicate a peak gain of 17.5 dBi and a maximum side-lobe level (SLL) of −13.5 dBi. Compared to conventional printed Yagi antennas of similar length, this integrated antenna offers wider bandwidth, higher gain, and lower SLL. It is particularly suitable for tunnel communication and radar detection systems.

1. INTRODUCTION

The rapid expansion of wireless communication systems has led to a growing demand for antennas with enhanced gain, broad bandwidth, and high radiation efficiency. Among various antenna designs, quasi-Yagi antennas stand out due to their high directivity, cost-effective fabrication, and compact form factor. Since the introduction of the Yagi antenna in 1929, numerous variants have been extensively developed and refined [1]. To further enhance performance, researchers have proposed various innovations and optimizations in multiple aspects [2–4].

Recent studies have shown that layout optimizations and structural refinements in Yagi antennas can extend their relative bandwidth by 20%–50% compared to conventional designs [5–7]. For example, a folded dipole feed mechanism enables dual-mode operation with multi-resonant impedance matching, achieving a peak gain exceeding 3.9 dB and a 20% fractional bandwidth in both modes [8]. Additionally, further miniaturization through substrate-integrated folded elements enhances the bandwidth to 48.7% while maintaining an average gain of 9.12 dBi [9]. However, challenges persist in suppressing side-lobe levels and ensuring gain uniformity across ultra-wideband operation.

Microstrip patches have been utilized to construct planar microstrip-line quasi-Yagi antennas [10–13]. In [14], a planar quasi-Yagi antenna incorporating parasitic pixelated strips was designed, featuring microstrip line feeding. Measurement results reveal that a single element achieves a 17.0% impedance bandwidth (covering 5.0–5.9 GHz) with a peak gain reaching 8.1 dBi. While printed Yagi antennas possess merits such as straightforward integration and structural compactness, their bandwidth nonetheless remains relatively constrained.

Integrating antennas with dielectric antennas has been explored to enhance their performance [15–21]. In [19], a long-fed Yagi antenna enclosed within a dielectric cover is proposed, effectively reducing the total length of the high-gain antenna. The design achieves a maximum gain of 18 dBi, a side-lobe level of −23.37 dB, and a relative bandwidth of 13.2%. While notable improvements in gain and side-lobe suppression have been achieved, the relative bandwidth remains limited, and the overall antenna size is relatively large.

In this paper, a conical printed Yagi antenna with broadband characteristics suitable for X-band applications is proposed. A dielectric cover is introduced around the Yagi antenna to effectively reduce the total length of the high-gain antenna. Additionally, a conical reflector and a conical dielectric cover are designed to enhance the radiation characteristics of the printed Yagi antenna in specific directions. As a result, within a footprint of $\lambda \times 1.9\lambda$, the proposed antenna achieves an impedance bandwidth of 62%, a side-lobe level (SLL) of −13.5 dBi, and a maximum gain of 17.5 dBi. A prototype is fabricated and measured, and the comparison between simulated and measured results demonstrates good agreement, validating the design methodology.

* Corresponding author: Yunqi Zhang (zhangyunqi@xupt.edu.cn).

2. BASIC ANTENNA STRUCTURE AND DESIGN

2.1. Design and Analysis of the Antenna

The designed antenna improves the active structure of the traditional Vivaldi antenna. First, the conventional feeder structure of the Vivaldi antenna is removed, and microstrip-line feeding is implemented. Then, to achieve impedance matching, metal patches of the antipodal Vivaldi antenna are printed on both sides of the dielectric substrate.

Better antenna radiation characteristics can be achieved when the length of the asymptote is equal to the dielectric wavelength. For an antipodal Vivaldi antenna, the opening width of the exponential asymptote is typically half of the corresponding dielectric wavelength at low frequencies [22]. Figure 1 illustrates the structure of the designed antipodal Vivaldi antenna. The complementary structure of the antipodal Vivaldi antenna is printed on an F4B dielectric substrate ($\varepsilon_r = 2.2$, $\tan\delta = 0.001$, $h = 0.5$ mm). The initial dimensions of the antenna are determined using Eq. (1) and Eq. (2), which define the coordinates of the inner and outer exponential asymptotic slot lines, respectively.

$$y_1 = a_1 e^{b_1 x_1} \tag{1}$$

$$y_2 = a_1 e^{b_2 x_2} + C \tag{2}$$

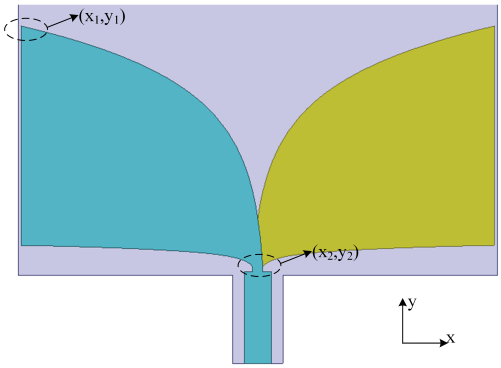

FIGURE 1. Structure of antipodal Vivaldi antennas.

All symbolic variables appearing in Eqs. (1) and (2) are defined in Table 1.

The technique of incorporating a curved director in front of the active array is employed to further enhance the antenna gain.

TABLE 1. Definition of symbolic variables.

Symbol	Definition	Unit
x_1, y_1	Horizontal and vertical coordinates of the outer exponential gradient curve	mm
x_2, y_2	Horizontal and vertical coordinates of the inner exponential gradient curve	mm
a_1	Initial amplitude parameter of the outer exponential gradient curve	mm
b_1, b_2	Curvature parameters of the outer and inner exponential gradient curves	/
C	Vertical offset constant of the inner exponential gradient curve	mm

Unlike a standard antipodal Vivaldi antenna, the director helps direct the electromagnetic waves from the antenna aperture toward the front of the dielectric substrate, resulting in minimal reflections and improved transmission characteristics. To evaluate its effectiveness, simulations are conducted for the antipodal Vivaldi antenna model with and without the loaded director, and the corresponding results are presented in Figure 2.

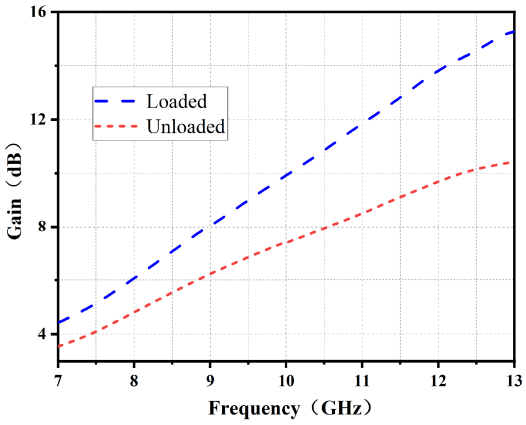

FIGURE 2. Gain plot with and without loaded director.

As shown in Figure 2, the antenna gain exhibits an increasing trend with rising frequency. In the low-frequency band of 6.9–9 GHz, the gain fluctuation is approximately 1.5 dB. This is because the energy of the Vivaldi antenna is primarily confined to excitation within the dielectric substrate and limited by the smaller radiation area, resulting in significantly reduced gain. Conversely, in the high-frequency band of 10–12.4 GHz, the antenna's slot-line structure is effectively excited, leading to an expansion of the radiation area, which substantially increases the gain compared to the low-frequency band [23].

It is also noted that with the addition of the director, the gain fluctuations in the low-frequency range are reduced, while a significant gain increase occurs in the high-frequency range (10–12.4 GHz). Without the director, the antipodal Vivaldi antenna exhibits a gain of 10 dBi at 12.4 GHz. However, with the director, the gain increases to 14.4 dBi, a substantial increase of 4.4 dBi. This demonstrates that the addition of a director can significantly enhance the antenna gain.

Generally, as the number of directors in a Yagi antenna increases, its gain also improves. With additional directors, the coupling of energy from the active element to the directors intensifies, enhancing the antenna's ability to radiate in the forward direction. However, the effectiveness of the directors diminishes once the number of directors exceeds a certain threshold. This is because increasing the number of directors causes the front end of the dielectric substrate to move further away from the active dipole.

When the printed Yagi antenna is operated at a high frequency of 13 GHz, the relationship between the number of directors N and radiation gain G is shown in Figure 3 for comparison. As seen in the figure, the antenna gain is 8.7 dB when no directors are added, and it increases as the number of directors increases. The gain reaches 15.3 dB when 11 directors are used. However, beyond this point, the gain increase slows down.

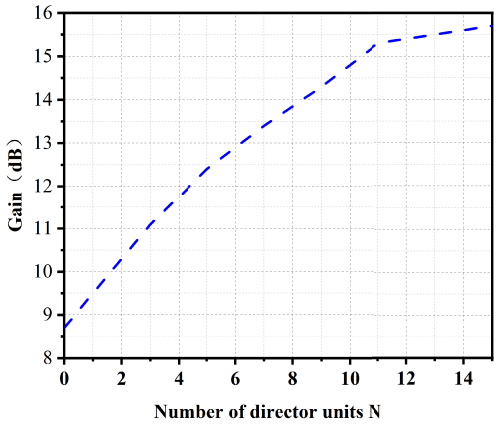

FIGURE 3. Antenna radiation gain versus the number of director units N.

This occurs because the director elements redirect the radiated energy through electromagnetic coupling. The first 11 elements are sufficient to effectively capture the vast majority of energy and focus it forward. However, the energy conversion efficiency drops sharply for any additional elements beyond this number. Concurrently, the spacing between directors approaches the half-wavelength critical value. When the number of elements exceeds 11, the path difference between the endmost director and the active dipole induces a phase reversal. This leads to the partial cancellation of energy due to opposing phases. Consequently, increasing the number of directors not only fails to proportionally enhance the gain but may also significantly enlarge the overall dimensions of the antenna system. Hence, this paper concludes that the optimal number of directors is 11.

In the final design of the printed Yagi antenna, the edge profile of the dielectric substrate features a linearly tapered gradient structure along the direction of maximum radiation, while maintaining a constant substrate thickness. This approach minimizes impedance mismatch issues caused by the substrate edges. Additionally, the curved shape of the active dipole mimics the exponential taper curvature of the Vivaldi antenna. This enables a traveling-wave current distribution and smooth impedance transition, thereby achieving high gain and low side lobes in the endfire radiation pattern. This design leverages the inherent broadband advantages of the Vivaldi antenna while enhancing endfire performance through structural optimization. The spacing between the active and passive dipoles is $0.1\lambda < r < 0.3\lambda$, while the spacing between the passive dipoles is $0.1\lambda < p < 0.4\lambda$. The finalized simulation model of the printed Yagi antenna is shown in Figure 4, and the dimensions are provided in Table 2.

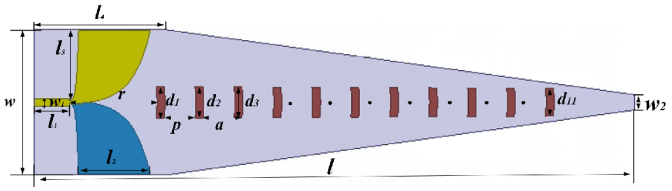

FIGURE 4. Structure of a printed Yagi antenna.

TABLE 2. Printed Yagi antenna dimensions.

Symbol	Value (mm)	Symbol	Value (mm)
l_1	5.3	d_2	6.4
l_2	25.5	d_3	6.4
l_3	90	d_4	6.3
l_4	15.9	d_5	6.2
w_1	3	d_6	6.1
w_2	28.5	d_7	6.0
l	1.6	d_8	5.9
p	6.7	d_9	5.8
a	1.5	d_{10}	5.7
r	12.5	d_{11}	5.6
d_1	6.4		

2.2. Reflector Design

Despite achieving a gain exceeding 15 dBi at high frequencies, the performance of the Yagi antenna remains suboptimal at low frequencies. As a result, improving its low-frequency gain has become a significant research challenge. In [27], an innovative approach is introduced that integrates a designed printed Yagi antenna with a metal reflector. This configuration enhances the directionality of the antenna radiation, focusing it more effectively along the $+X$-axis. As a result, the design modification narrows the main lobe width and increases the gain of the printed Yagi antenna, as shown in Figure 5.

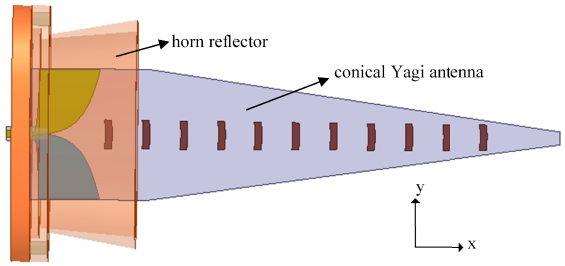

FIGURE 5. Printed Yagi antenna model loaded with cylindrical reflector.

The antenna consists primarily of a printed Yagi antenna embedded in a metal reflector. The active dipole of the printed Yagi antenna is positioned approximately 1/4 wavelength away from the reflector. The metal reflector is hollow, and the bottom of the reflector features a rectangular groove used to secure the structure of the printed Yagi antenna. Figure 6 compares the simulated gain performance of the printed Yagi antenna with and without the metal reflector.

From Figure 6, it can be observed that the gain at low frequencies significantly increases with the addition of a metal reflector, rising from 4.5 dB to 10 dB at 7.4 GHz, an improvement of 5.5 dB. This increase is primarily due to the metal reflector acting as a reflecting plate, redirecting the energy that would have been radiated backward by the printed Yagi antenna forward. This method greatly improves the antenna's radiation efficiency, minimizing energy wastage. However, the change at

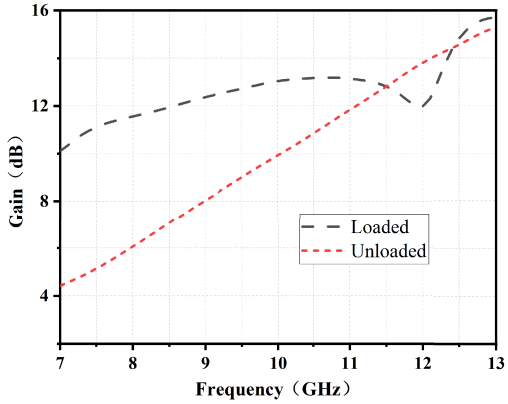

FIGURE 6. Comparison of gains with and without loaded reflector.

high frequencies is less significant, and the gain does not continue to increase after the reflector is added. At a frequency of 11.9 GHz, the observed gain reduction is mainly attributed to internal reflections within the metallic cavity after the introduction of the metal reflector, which leads to energy dissipation. Nevertheless, the overall effect of the reflector is positive, resulting in an improvement in gain.

The performance of an antenna is also influenced by the shape of the metal reflector. To investigate this effect, gain simulations were conducted for both flared and cylindrical metal reflector configurations using High-Frequency Structure Simulator (HFSS). The comparative results are shown in Figure 7.

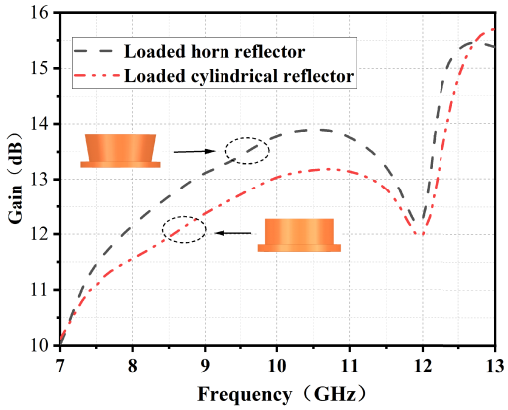

FIGURE 7. Comparison of gain between loaded horn reflector and loaded cylindrical reflector.

As shown in Figure 7, the horn reflector demonstrates higher gain than the cylindrical reflector within the operational frequency band. At 7 GHz, the low-frequency gains of the two reflectors are equal. As the frequency increases, the horn reflector provides better gain, with the maximum gain difference reaching 0.8 dB at 10.5 GHz. However, as the frequency continues to increase, the gain of both reflectors decreases. When the frequency exceeds 12 GHz, the gain of both reflectors gradually increases again.

The final model of the reflector, shown in Figure 8, is made of aluminum and features an internally hollow structure. The dimensions of the horn reflector were determined through simulations, and the specific values are provided in Table 3.

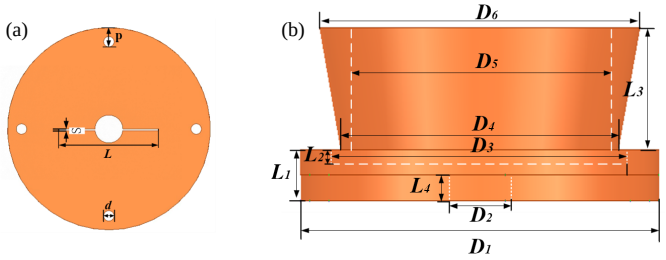

FIGURE 8. Horn reflector model. (a) Back. (b) Front.

TABLE 3. Dimensions of horn reflectors.

Symbol	Value (mm)	Symbol	Value (mm)
D_1	56	L_2	1
D_2	8	L_3	20
D_3	43.4	L_4	2
D_4	50	d	3
D_5	19	L	28.5
D_6	58	S	0.5
L_1	4	P	5.5

The radiation patterns of the printed Yagi antenna were simulated at frequencies of 7, 8, 9, 10, 11, 12, and 13 GHz in both the E-plane and H-plane configurations after incorporating a metal reflector. The simulation results are shown in Figure 9.

The radiation pattern indicates a gradual increase in gain with rising frequency, with a slight reduction at 12 GHz before continuing to increase beyond this point. At the low frequency of 7 GHz, it is observed that there is no side-lobe level (SLL) in the H-plane directional diagram. As the frequency increases, the SLL gradually rises. At 13 GHz, the antenna exhibits the highest SLL, reaching 8.3 dB. Meanwhile, the E-plane directional diagram shows that the SLL is relatively small in the frequency range from 7 GHz to 12 GHz. At 13 GHz, the highest SLL is observed, reaching -2.5 dB.

Thus, it is evident that the printed Yagi antenna exhibits stable performance across a wide bandwidth and can meet the requirements for directional radiation. However, it also has the disadvantage of high SLL at higher frequencies.

2.3. Design and Analysis of Dielectric Rods

Based on the above study, it is evident that although the printed Yagi antenna achieves broadband high gain, the SLL remains relatively high, particularly at higher frequencies. Therefore, reducing the SLL of the printed Yagi antenna becomes a crucial task. As well known, a dielectric rod can cause the outwardly dispersing wave beam to converge, allowing the wave traveling along the medium to gradually transition from a bound wave to a free-space wave, resulting in high gain and reduced SLL.

Figure 10 illustrates the broadband printed Yagi antenna loaded with a cylindrical dielectric rod, primarily designed to reduce high-frequency SLL and improve gain. In this configuration, the printed Yagi antenna is placed inside a hollow cylindrical dielectric rod. The dielectric substrate of the printed Yagi antenna is linearly tapered, and the bottom of the antenna is loaded with a flared metal reflector to further increase the gain.

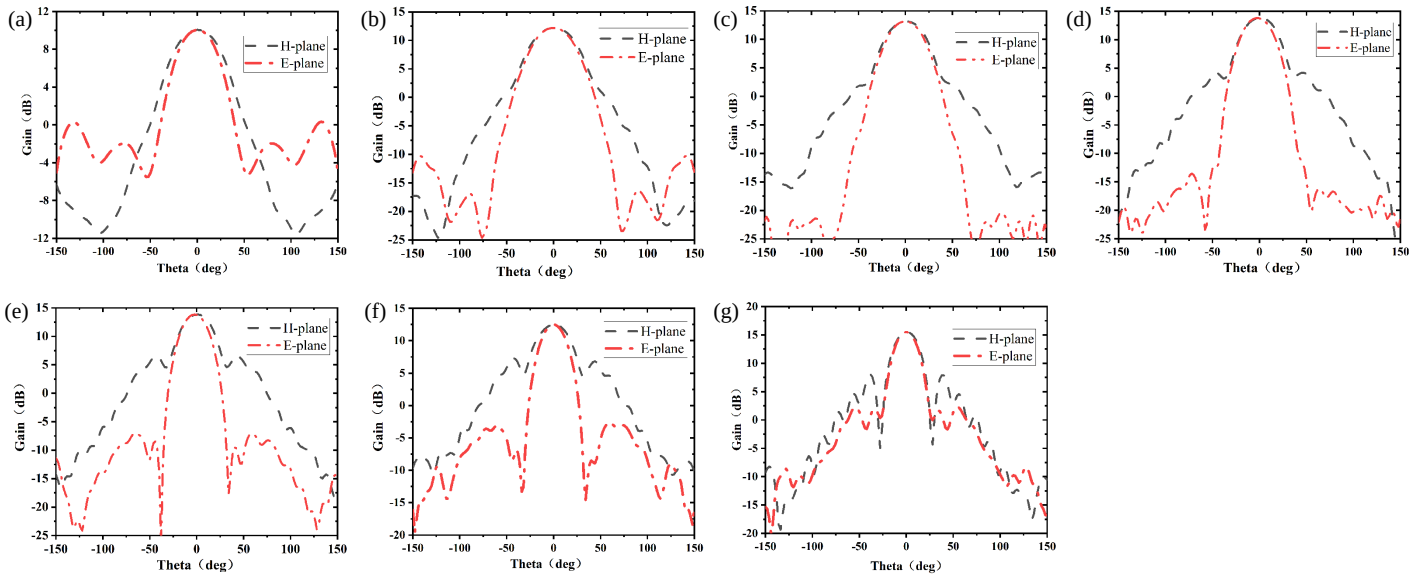

FIGURE 9. Radiation direction of the E/H plane of the printed Yagi antenna at 7–13 GHz. (a) 7 GHz, (b) 8 GHz, (c) 9 GHz, (d) 10 GHz, (e) 11 GHz, (f) 12 GHz, (g) 13 GHz.

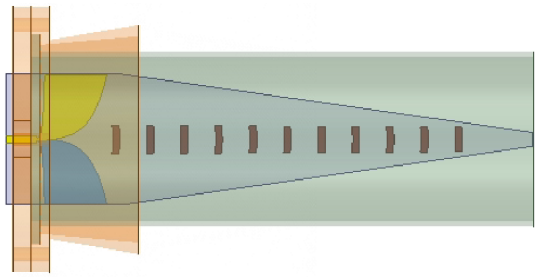

FIGURE 10. Broadband printed Yagi antenna loaded with cylindrical dielectric rods.

To validate the hypothesis that incorporating a dielectric rod enhances antenna gain while suppressing high-frequency side-lobe levels (SLLs), simulations were conducted both with and without a cylindrical dielectric rod at an operating frequency of 13.2 GHz. The comparative results are shown in Figure 11.

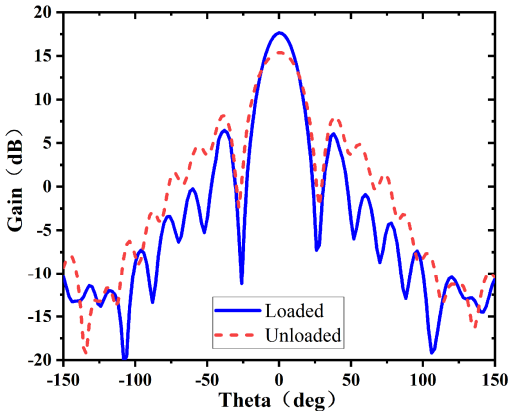

FIGURE 11. Plot of simulation results with and without loading cylindrical dielectric rods.

Without the dielectric rod, the antenna gain is 15.3 dBi, which increases to 16.5 dBi when the dielectric rod is added, resulting in a total gain improvement of 0.8 dBi. This indicates that the addition of the dielectric rod enhances both the gain and radiation directional pattern of the printed Yagi antenna while maintaining the same overall size.

Furthermore, Figure 11 shows that the unloaded Yagi antenna has a higher SLL of −7.2 dB. However, when the cylindrical dielectric rod is introduced, the SLL decreases to −11 dB. This reduction confirms that loading the antenna with a dielectric rod effectively enhances gain and suppresses SLL.

Loading a cylindrical dielectric rod can enhance antenna gain, but the radiation characteristics vary with the rod's shape profile. To further optimize the radiation performance, we experimented with dielectric rods of different shapes and conducted a comparative performance analysis. The rod types employed in the experiments include stepped, tapered, triangular-wave periodic, and cylindrical ones, with their specific profiles illustrated in Figure 12.

Figure 13 presents the simulation results of four differently profiled dielectric rods operating at 13.2 GHz. The analysis reveals that the tapered dielectric rod, owing to its gradient structure, facilitates a smoother electromagnetic wave transition from the dielectric to free space. This effect effectively reduces reflection loss and focuses energy in the main lobe direction, ultimately achieving a high gain of 17.5 dBi while suppressing the SLL to −13.5 dBi. In contrast, although the stepped configuration yields higher gain, its side-lobe performance degrades significantly. Both the cylindrical and triangular-wave periodic structures underperform the tapered rod in terms of gain and side-lobe suppression. Considering the overall performance balance, the tapered dielectric rod was selected to enhance gain and reduce side lobes.

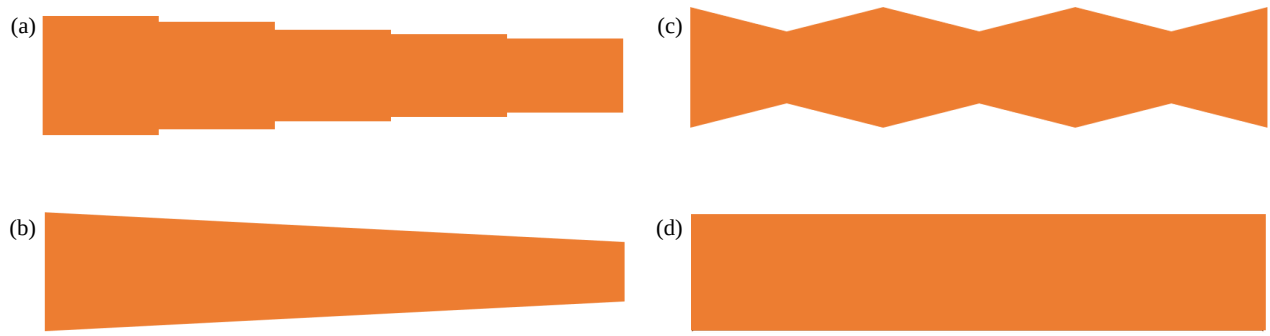

FIGURE 12. Shape of dielectric rods. (a) Stepped dielectric rod. (b) Tapered dielectric rod. (c) Trigonometric dielectric rod. (d) Cylindrical dielectric rod.

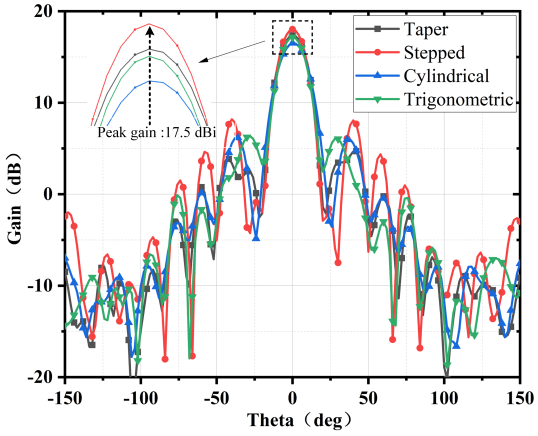

FIGURE 13. Simulation results of gain for different dielectric rods.

Side lobe suppression primarily benefits from the energy focusing effect occurring during wave propagation through media with different permittivities. Furthermore, as the rod profile gradually narrows, the structure's directivity increases, effectively mitigating reflections caused by abrupt terminations. The adopted tapered dielectric rod model, fabricated from low-loss Teflon material (relative permittivity $\varepsilon = 2.1$), is illustrated in Figure 14.

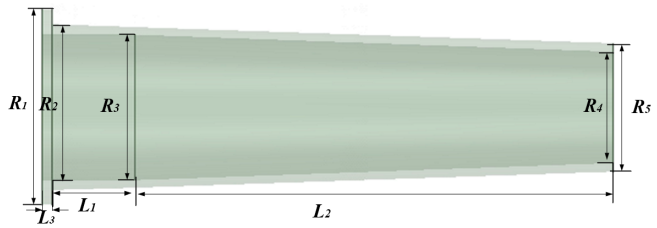

FIGURE 14. Tapered dielectric rod model.

Although the tapered dielectric rod can reduce the side-lobe level (SLL), a smaller size is not always better. To ensure the dielectric rod operates in the fundamental mode, its maximum diameter ($D_{\max}$) must satisfy the condition given in Eq. (3), and its minimum diameter ($D_{\min}$) must satisfy the condition in Eq. (4). Here, ε_{r2} represents the relative permittivity of the dielectric rod.

TABLE 4. Media rod dimensions.

Symbol	Value (mm)	Symbol	Value (mm)
R_1	46	R_5	36
R_2	38	L_1	18
R_3	34	L_2	92
R_4	32	L_3	2

After optimization using HFSS software, the final dimensions of the dielectric rod are provided in Table 4.

$$D_{\max} = \frac{\lambda_0}{\sqrt{\pi\left(\varepsilon_{r2}-1\right)}} \tag{3}$$

$$D_{\min} = \frac{\lambda_0}{\sqrt{2.5\pi\left(\varepsilon_{r2}-1\right)}} \tag{4}$$

3. ANTENNA OVERALL STRUCTURE SIMULATION AND ACTUAL MEASUREMENT

The preceding section detailed the design process for a printed Yagi antenna, a flared metal reflector, and a tapered dielectric rod. By integrating these components, we developed a broadband, high-gain, low-SLL printed Yagi antenna tailored for X-band applications. The structural diagram of the designed antenna is presented in Figure 15. The distance from the feed port to the reflector is denoted as d, and the impedance bandwidth can be adjusted by modifying the size of d. The overall dimensions of the antenna are 117 mm × 58 mm × 58 mm, and the antenna is both easy to design and low in cost.

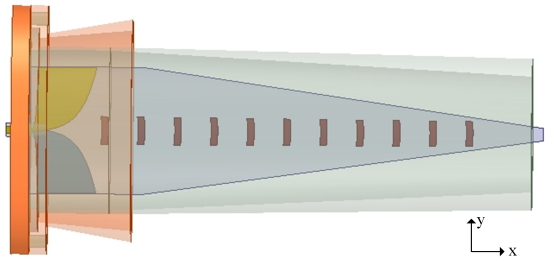

FIGURE 15. Antenna simulation structure.

Based on the antenna structure schematic and the optimized dimensions provided earlier, a prototype of the printed Yagi antenna was fabricated. The antenna ports were fitted with SMA connectors to facilitate power feeding. Subsequently, the performance of the manufactured antenna samples was evaluated to validate both the design approach and the accuracy of the simulation results for the broadband, high-gain, low-profile printed Yagi antenna proposed in this paper.

Figure 16 presents the physical drawings of the components of the designed antenna, which primarily include the printed Yagi antenna, tapered dielectric rod, and flared metal reflector. The printed Yagi antenna is fabricated using Printed Circuit Board (PCB) technology, while the dielectric rod and reflector are fabricated using 3D printing technology. All components are integrated to form a broadband, high-gain, low-SLL printed Yagi antenna for X-band applications.

FIGURE 16. Printed Yagi antenna processing diagram.

Clearly, the structure and fabrication process of this printed Yagi antenna are simple, offering significant advantages for engineering applications.

Using a vector network analyzer, we obtained the $|S_{11}|$ parameters of the antenna, and its amplitude profile is shown in Figure 17. The results demonstrate that the measured -10 dB impedance bandwidth of the antenna is 62% (6.9–13.1 GHz), while the simulation results indicate a -10 dB impedance bandwidth of 63% (6.9–13.2 GHz). The experimental results show good consistency with the simulation ones, verifying the reliability and validity of the design. The primary target band covered by this antenna is the X-band (8–12 GHz), making it highly suitable for high-gain applications within the X-band frequency range.

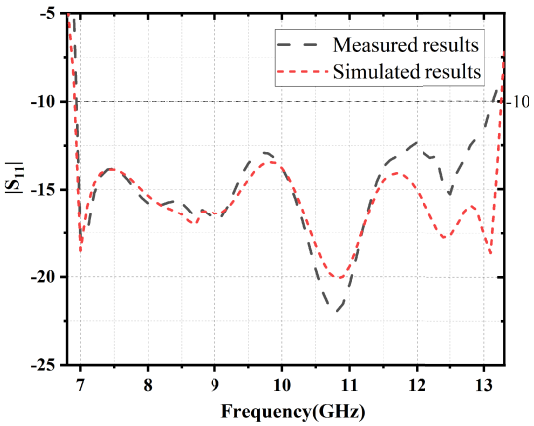

FIGURE 17. Simulated and measured results of antenna $|S_{11}|$.

Using the near-field measurement system, we obtained normalized radiation patterns of the antenna at 7, 8, 9, 10, 11, 12, 13, and 13.2 GHz for both the measured and simulated E-plane and H-plane configurations. The measurement photograph and results are shown in Figures 18 and 19, respectively.

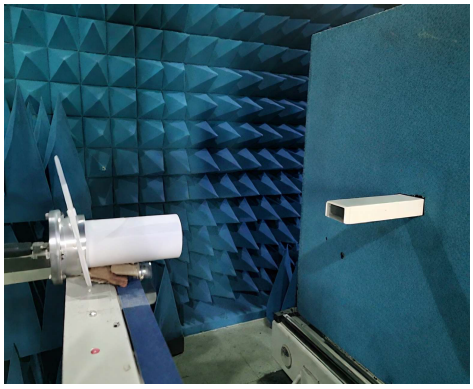

FIGURE 18. Near-field measurement environment.

From the figures, it can be observed that, at the iso-frequency points of 7–9 GHz, the beam exhibits a pencil-like shape with good directionality, a wider beam, and no obvious side-lobe level (SLL). As the frequency increases, the directionality improves in both the middle and high-frequency bands; the beam narrows; and the gain increases, but the SLL also rises. At the high operational frequency of 13.2 GHz, the antenna shows its highest SLL in the E-plane and H-plane, reaching -18 dB and -13.5 dB, respectively. This phenomenon is primarily due to the excitation of high-frequency waves by the narrow end of the slot line. When the substrate thickness matches the width of the slot line and operates at such high frequencies, the electromagnetic wavelength decreases. As a result, the conduction region of the feed portion becomes relatively elongated, leading to increased dielectric loss. These dual losses contribute to reduced energy directionality towards the end-fire orientation.

By comparing the E-plane and H-plane radiation patterns, it is evident that the SLL in the H-plane consistently exceeds the SLL in the E-plane, regardless of whether the antenna operates at high or low frequencies. This discrepancy is mainly due to the excessive radiation from both sides of the dielectric substrate. Additionally, the antenna's cross-polarization values are -29.5 dB, -23 dB, and -19.5 dB at 7 GHz, 10 GHz, and 13 GHz, respectively. These values indicate that the antenna's main polarization is stronger, resulting in more efficient radiated energy.

Table 5 presents a comparison between the antenna designed in this paper and those from related literature. In [24], a printed Yagi antenna is proposed that uses consumable dielectrics to achieve high gain by loading a double-helix antenna within a dielectric antenna. However, it has a relatively small size and a narrow impedance bandwidth of only 6%. Moreover, the antenna gain is quite low, at just 9.5 dBi.

In comparison, [25] introduces an innovation in reducing side-lobe level (SLL). This antenna achieves dual-polarized feeding using a square metal waveguide and a conical horn. While the SLL reaches -25 dB, the antenna's structure is more

TABLE 5. Antenna performance comparison.

Literature	Polarization Mode	Frequency (GHz)	Impedance Bandwidth (%)	Peak Gain (dBi)	SLL (dB)	Size (λ_0^2)
[8]	Single polarization	23–28	20	4.9	/	0.56×1.6
[19]	Single polarization	8.5–9.7	13.2	18	-23.37	7.7×0.9
[25]	Single polarization	23.5–24.5	7	11.5	-25	7.7×0.9
[26]	Dual polarization	3.1–10.6	8/7	11.5	-25	8×4.5
[27]	Single polarization	26.45–29.25	10	9.45	/	/
This paper	Single polarization	6.9–13.1	63	17.5	-13.5	4×1.9

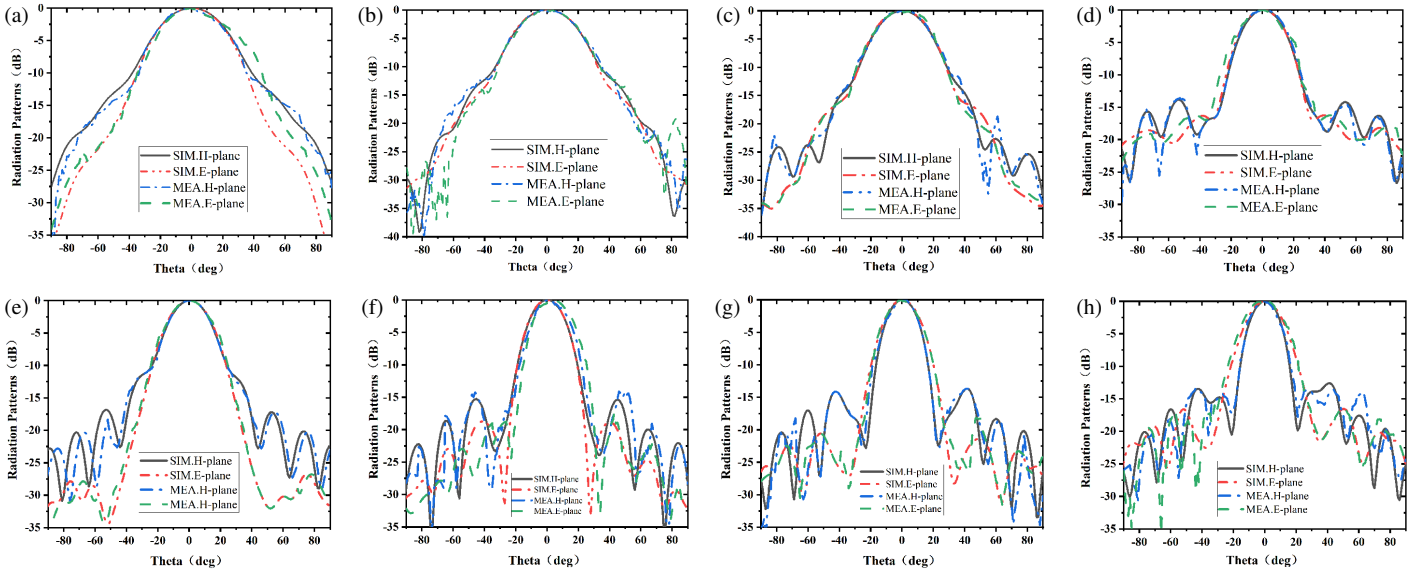

FIGURE 19. Simulated and measured radiation directions of printed Yagi antenna. (a) 7 GHz, (b) 8 GHz, (c) 9 GHz, (d) 10 GHz, (e) 11 GHz, (f) 12 GHz, (g) 13 GHz, (h) 13.2 GHz.

complex and larger, and the impedance bandwidths of the dual ports are still very narrow at 7% and 8%, respectively, limiting its practical use. Ref. [19] proposes a printed Yagi antenna featuring high gain and low side-lobe characteristics. This design integrates a printed Yagi antenna with a dielectric rod, achieving a peak antenna gain of up to 18 dBi, with the highest side-lobe level at -23 dB. However, it suffers from a narrow impedance bandwidth of 13.2%, and the overall dimensions of the antenna are relatively large.

The antenna proposed in this paper implements multidimensional optimizations based on the design foundation of [19]. In terms of radiating element design, a antipodal Vivaldi curved-gradient dipole is adopted as the active unit. Its exponentially tapered slotline structure significantly expands the impedance bandwidth to 63% by exciting a multi-resonance traveling-wave radiation mechanism (representing a 4.8-fold improvement over the 13.2% in [19]). The cylindrical reflector of [19] is replaced with a tapered horn-shaped metallic reflector, which reconstructs backward radiation energy through a tilted cavity structure to enhance mid-band gain. By optimizing the dielectric rod profile, the discrete triangular periodic structure is upgraded to a continuous linear gradient, achieving smooth electromagnetic wave transition from dielectric to free space, thereby increasing gain and suppressing side lobes. The final antenna exhibits characteristics of wide bandwidth, compact structure, high gain, and low SLL, achieving breakthroughs in both comprehensive performance and engineering practicality.

4. CONCLUSIONS

This paper presents a broadband, high-gain, low SLL printed Yagi antenna designed for X-band operation. The antenna consists of three primary components: a broadband printed Yagi antenna element, a flared metallic reflector, and a tapered dielectric rod. The broadband characteristic is achieved by using an antipodal Vivaldi element as the active dipole, while the gain is enhanced by incorporating 11 parasitic director dipoles positioned in front of the active dipole. To improve the gain at low frequencies, a horn-type reflector is added at the feed, ensuring stable gain across the entire frequency band. Additionally, a tapered dielectric rod is positioned at the outermost side, further increasing the antenna's gain while reducing the side-lobe level (SLL).

The antenna demonstrates a compact size, wide bandwidth, high gain, low SLL, stable radiation direction, and excellent end-to-end radiation performance, all within a simple structure that is easy to fabricate. These characteristics make it suitable for practical applications. To validate the performance stability

and reliability, the antenna prototype was fabricated and tested. After data collection and analysis, the measured results closely match the simulated ones, confirming the antenna's design effectiveness. Comparative analysis with similar antenna structures shows that the proposed antenna outperforms others in key areas, highlighting its advantages in terms of both performance and design simplicity.

ACKNOWLEDGEMENT

This work is supported in part by Scientific Research Program Funded by Shaanxi Provincial Education Department (22JC058 24JR154) and Technology Innovation Leading Program of Shaanxi (Program No. 2024ZC-YYDP-33).

REFERENCES

[1] Yagi, H. and S. Uda, "Projector of the sharpest beam of electric waves," *Proceedings of the Imperial Academy*, Vol. 2, No. 2, 49–52, 1926.

[2] Li, D., C. Yang, L. Shi, Y. Liu, Q. Chen, and N. Shinohara, "A high-gain filtering quasi-Yagi antenna based on compressed third-order mode dipole," *IEEE Antennas and Wireless Propagation Letters*, Vol. 23, No. 10, 2860–2864, 2024.

[3] Fan, F.-F., Q.-L. Chen, Y.-X. Xu, X.-F. Zhao, J.-C. Feng, and Z.-H. Yan, "A wideband compact printed dipole antenna array with SICL feeding network for 5G application," *IEEE Antennas and Wireless Propagation Letters*, Vol. 22, No. 2, 283–287, 2023.

[4] Alekseytsev, S. A. and A. P. Gorbachev, "The novel printed dual-band quasi-Yagi antenna with end-fed dipole-like driver," *IEEE Transactions on Antennas and Propagation*, Vol. 68, No. 5, 4088–4090, 2020.

[5] Zhang, D. and Q. Wu, "A shared-aperture antenna with high-aperture reuse efficiency and high isolation based on the quasi-Yagi structure," *IEEE Transactions on Antennas and Propagation*, Vol. 71, No. 11, 8504–8513, 2023.

[6] Huang, W., L.-Y. Ji, and S.-G. Zhou, "Multiband modified Yagi antenna in a shared transverse aperture," *IEEE Antennas and Wireless Propagation Letters*, Vol. 23, No. 9, 2583–2587, 2024.

[7] Shirabadagi, S. S. and V. G. Kasabegoudar, "A planar suspended multiband Yagi antenna for WLAN, LTE, and 5G wireless applications," *Progress In Electromagnetics Research C*, Vol. 122, 141–151, 2022.

[8] Ha, N., G. Kim, N. S. Jeong, and S. Kim, "Design of mmWave foldable vertically stacked Yagi-Uda antenna inspired by Origami and Kirigami theories," *IEEE Antennas and Wireless Propagation Letters*, Vol. 21, No. 8, 1634–1638, 2022.

[9] Chen, Y., J. Shi, K. Xu, L. Lin, and L. Wang, "A compact wideband quasi-Yagi antenna for millimeter-wave communication," *IEEE Antennas and Wireless Propagation Letters*, Vol. 22, No. 6, 1481–1485, 2023.

[10] Li, D., C. Yang, Y. Liu, L. Yang, and Q. Chen, "Planar printed wideband filtering quasi-Yagi antenna and its notch-band design using parasitic elements for vehicular communication," *IEEE Transactions on Vehicular Technology*, Vol. 73, No. 2, 2122–2131, 2024.

[11] Hwang, M., G. Kim, S. Kim, and N. S. Jeong, "Origami-inspired radiation pattern and shape reconfigurable dipole array antenna at C-band for cubesat applications," *IEEE Transactions on Antennas and Propagation*, Vol. 69, No. 5, 2697–2705, 2021.

[12] Nella, A., V. Dhasarathan, J. Kříž, T. Addepalli, S. Hubálovský, and M. Sharma, "A novel conformal quasi-Yagi antenna with offset feed for high directional 300 GHz applications," *IEEE Access*, Vol. 11, 37 335–37 346, 2023.

[13] Wang, J., Z. Huang, C. Wang, G. Cheng, G. Xu, W. Wang, Y. Li, L. Yang, and X. Wu, "Theoretical analysis and applications for the element-rotation-based circularly polarized Yagi-Uda antenna," *IEEE Transactions on Antennas and Propagation*, Vol. 71, No. 11, 9018–9023, 2023.

[14] Bi, J., F. Qin, C. Gu, and H. Zhang, "A wideband multibeam planar quasi-Yagi array antenna based on parasitic pixel strips," *IEEE Antennas and Wireless Propagation Letters*, Vol. 24, No. 7, 2124–2128, 2025.

[15] Zambak, M. F., S. Johari, M. N. M. Yassin, A. M. Ismail, and A. Alghaihab, "Ultra-wide band antipodal Vivaldi antenna using metasurface lens for gain and front-to-back ratio (FBR) improvement," *Radio Science*, Vol. 59, No. 10, 1–15, 2024.

[16] Tian, Z., J. Zhang, and S. Yi, "Innovative W-band through-wall radar with sector scanning: Utilizing traveling wave tubes for enhanced penetration," *IEEE Sensors Journal*, Vol. 24, No. 19, 30 801–30 809, 2024.

[17] Ponti, C., S. Ceccuzzi, P. Baccarelli, and G. Schettini, "A resonant-cavity antenna with high-gain and wide bandwidth with an all-dielectric 3D-printed superstrate," *IEEE Access*, Vol. 12, 111 982–111 991, 2024.

[18] Fakhte, S. and L. Matekovits, "Enhancing the radiation pattern of circularly polarized dielectric rod antenna using planar excitation method," *IEEE Access*, Vol. 11, 125 109–125 121, 2023.

[19] Nasir, M., Y. Xia, M. Jiang, and Q. Zhu, "A novel integrated Yagi-Uda and dielectric rod antenna with low sidelobe level," *IEEE Transactions on Antennas and Propagation*, Vol. 67, No. 4, 2751–2756, 2019.

[20] Chaparala, R., S. Imamvali, S. Tupakula, K. Prakash, S. Bansal, M. M. Ismail, and A. J. A. Al-Gburi, "Spoof surface plasmon polaritons-based feeder for a dielectric rod antenna at microwave frequencies," *Progress In Electromagnetics Research M*, Vol. 129, 23–32, 2024.

[21] Baldazzi, E., A. Al-Rawi, R. Cicchetti, A. B. Smolders, and D. Caratelli, "A high-gain dielectric resonator antenna with plastic-based conical horn for millimeter-wave applications," *IEEE Antennas and Wireless Propagation Letters*, Vol. 19, No. 6, 949–953, 2020.

[22] Gazit, E., "Improved design of the Vivaldi antenna," in *IEE Proceedings H (Microwaves, Antennas and Propagation)*, Vol. 135, No. 2, 89–92, Apr. 1988.

[23] Zhou, Q., J. Zhang, X. Zheng, J. Zhang, Z. Zhang, and L. Huang, "A high-gain antipodal Vivaldi antenna operating at 1 GHz to 40 GHz for photonic-assisted receiver," *IEEE Antennas and Wireless Propagation Letters*, Vol. 23, No. 10, 3068–3072, 2024.

[24] Chen, P., R. Meng, and Q. Zhu, "Design of compact high-gain dielectric rod antennas and arrays in lossy medium," *Microwave and Optical Technology Letters*, Vol. 55, No. 10, 2277–2282, 2013.

[25] Sporer, M., R. Weigel, and A. Koelpin, "A 24 GHz dual-polarized and robust dielectric rod antenna," *IEEE Transactions on Antennas and Propagation*, Vol. 65, No. 12, 6952–6959, 2017.

[26] Nguyen, P. T., A. Abbosh, and S. Crozier, "Wideband and compact quasi-Yagi antenna integrated with balun of microstrip to slotline transitions," *Electronics Letters*, Vol. 49, No. 2, 88–89, 2013.

[27] Esmail, B. A. F., D. Isleifson, and S. Koziel, "Millimeter-wave Yagi MIMO antenna with high isolation and beam-tilting capability using optimized metamaterials," *IEEE Access*, Vol. 13, 107 710–107 719, 2025.